A three-dimensional scaffold with precise micro-architecture and surface micro-textures

Alvaro Mata [a,b,1,2], Eun Jung Kim [a,1], Cynthia A. Boehm [a,c,1,3], Aaron J. Fleischman [a,1], George F. Muschler [a,c,1,3], Shuvo Roy [a,d,*,1]

[a] Department of Biomedical Engineering, Lerner Research Institute, Cleveland Clinic, 9500 Euclid Avenue, Cleveland, OH 44195, United States
[b] Nanotechnology Platform, Parc Científic Barcelona, Baldiri Reixac 10, 08028 Barcelona, Spain
[c] Department of Orthopaedic Surgery, Cleveland Clinic, 9500 Euclid Avenue, Cleveland, OH 44195, United States
[d] Department of Bioengineering & Therapeutic Sciences, University of California, San Francisco, Byers Hall, Room 203A, MC 2520, 1700 4th Street, San Francisco, CA 94158, United States

ARTICLE INFO

ABSTRACT

A three-dimensional (3D) structure comprising precisely defined micro-architecture and surface micro-textures, designed to present specific physical cues to cells and tissues, may provide an efficient scaffold in a variety of tissue engineering and regenerative medicine applications. We report a fabrication technique based on microfabrication and soft lithography that permits for the development of 3D scaffolds with both precisely engineered architecture and tailored surface topography. The scaffold fabrication technique consists of three key steps starting with microfabrication of a mold using an epoxy-based photoresist (SU-8), followed by dual-sided molding of a single layer of polydimethylsiloxane (PDMS) using a mechanical jig for precise motion control; and finally, alignment, stacking, and adhesion of multiple PDMS layers to achieve a 3D structure. This technique was used to produce *3D Texture* and *3D Smooth* PDMS scaffolds, where the surface topography comprised 10 μm diameter/height posts and smooth surfaces, respectively. The potential utility of the 3D microfabricated scaffolds, and the role of surface topography, were subsequently investigated *in vitro* with a combined heterogeneous population of adult human stem cells and their resultant progenitor cells, collectively termed connective tissue progenitors (CTPs), under conditions promoting the osteoblastic phenotype. Examination of bone-marrow derived CTPs cultured on the *3D Texture* scaffold for 9 days revealed cell growth in three dimensions and increased cell numbers compared to those on the *3D Smooth* scaffold. Furthermore, expression of alkaline phosphatase mRNA was higher on the *3D Texture* scaffold, while osteocalcin mRNA expression was comparable for both types of scaffolds.

© 2009 Elsevier Ltd. Open access under CC BY-NC-ND license.

1. Introduction

There is an increasing need to design and develop materials, devices, and cell therapies that can repair human tissues and organs [1]. To this end, both *in vivo* and *in vitro* approaches to control cell growth and engineer functional tissues have recently been recognized to offer tremendous potential [2]. Tissue engineering and regenerative medicine applications are strongly dependent on having a bioactive three-dimensional (3D) scaffold that deliberately recruits, specifically stimulates, and effectively guides cells to form tissues and organs [3]. The importance of both the scaffold's biochemical and physical properties has been recognized, and the aim has been to tailor them to elicit specific biological responses [3,4]. Nonetheless, one of the major difficulties in achieving functional engineered tissues has been, and still is, the successful generation of reproducible scaffolds with specific and desired properties that are able to recreate and control the complex cellular microenvironment [3,4].

Physical characteristics of the scaffold, defined by the micro-architecture (porosity, pore geometry, interconnectivity) and the surface micro-textures (surface topography), are known to extensively influence cell function [5] and play a crucial role in tissue regeneration [6–8]. The scaffold micro-architecture significantly affects the development and function of specific tissues, by providing

* Corresponding author. Department of Bioengineering & Therapeutic Sciences, University of California, San Francisco, Byers Hall, Room 203A, MC 2520, 1700 4th Street, San Francisco, CA 94158, United States. Tel.: +1 415 514 9666; fax: +1 415 514 9766.
 E-mail address: shuvo.roy@ucsf.edu (S. Roy).
[1] Tel.: +1 216 445 3243; fax: +1 216 444 9198.
[2] Tel.: +34 93 403 48 80; fax: +34 93 403 71 09.
[3] Tel.: +1 216 444 5338; fax: +1 216 444 9198.

a 3D space that determines the spatial organization and nutritional conditions of cells [7,9]. For many tissues, an ideal scaffold micro-architecture should be highly porous [9] with interconnected pores of defined diameters (for example of ~200–900 μm in diameter in the case of bone [10,11]) and exhibits high surface area-to-volume ratio [9,12] to allow high rates of mass transfer [9], cell in-growth, and vascularization [3,6,13]. Unfortunately, traditional scaffold fabrication techniques like solvent casting and particulate leaching are limited in their ability to provide well-controlled and repro-ducible micro-architectures [3,14–16]. To overcome this limitation, novel techniques such as fused deposition modeling, 3D printing, micro-stereolithography, and microfabrication have been applied towards the fabrication of scaffolds [6,14–22]. Although these tech-niques have successfully produced scaffolds with more precise micro-architectures, they are limited in their ability to incorporate precise surface micro-textures [22], which are known to significantly affect cell behavior [23–25].

Microfabrication and related MEMS (microelectromechanical systems) production techniques such as soft lithography [26] offer the precision and reproducibility to produce pre-defined surface micro-textures that can systematically interact with cells and tissues [24,27]. The inherent precision of microfabrication allows small geometrical modifications of the surface features to better identify and quantify specific effects on cell behavior such as attachment, orientation, migration, proliferation, protein produc-tion, and differentiation on a variety of cells [24–31]. Control and reproducibility of this topographically based cell stimulation may be used therapeutically to elicit desired biological responses. We have previously reported on the effects of various micro-textures on Connective Tissue Progenitors (CTPs) [29,30,32]. These primary cells denote a combined heterogeneous population of stem cells and progenitor cells that are resident in native tissue, and capable of proliferating and differentiating into connective tissue pheno-types [33–35]. In particular, our investigations showed that 10 μm diameter/height posts patterned on two-dimensional (2D) Poly-dimethylsiloxane (PDMS) substrates selectively enhanced in vitro CTP (and their progeny) growth relative to smooth PDMS surfaces, under identical culture conditions promoting osteoblastic pheno-type [30,32]. However, the practicality of this approach to engineer 3D tissues would require the incorporation of such topographical features within a 3D scaffold.

The use of microfabrication techniques to develop 3D micro-architectures with surfaces that include bioactive micro-textures is hindered by the inherent 2D fabrication characteristics of tradi-tional photolithography-based processes [3,26]. Consequently, we have developed a novel 3D production technique that combines microfabrication and soft lithography to construct 3D scaffolds with precise pore geometry, porosity, and surface topography that are designed to guide and selectively stimulate cells and tissues with potential use in both tissue engineering and regenerative medicine. This strategy aims to create highly biomimetic and bioactive microenvironments through modulation of the physical properties (pore geometry, porosity, and surface topography) of the scaffold. While this fabrication technique can be used to develop scaffolds for the growth of a variety of cells and tissues, here we describe the fabrication of 3D scaffolds and their effect on the in vitro behavior of human CTPs (and their progeny) cultured under conditions promoting osteoblastic phenotype.

2. Materials and methods

2.1. 3D scaffold fabrication

The 3D scaffolds were produced through an innovative technique that combined microfabrication and soft lithography, and consisted of the dual-sided molding and stacking of PDMS layers (Fig. 1) [36]. The unique feature of the current scaffold fabrication technique is that it allows for the construction of pre-defined and precise micro-architectures and surface micro-textures. Although studies have revealed bone tissue penetration in pore sizes from 200 to 900 μm in diameter, most bone in-growth has been observed in pore diameters that are in the range of 300–500 μm [11]. Therefore, we selected to fabricate scaffolds with 300 μm diameter meandering vertical pores and 200 μm × 400 μm horizontal pores, which should enhance cell penetration, and extracellular matrix production [6,11]. In addition, every horizontal surface within the scaffold comprised 10 μm diameter and 10 μm high posts (with 10 μm separation) as this pattern was shown to enhance CTP growth in vitro [30,32].

2.1.1. Mold fabrication

First, a multilevel SU-8 photoresist (MicroChem Corp., Newton, MA) process was developed to produce SU-8 molds incorporating holes and posts of various dimensions [37]. SU-8 is a high contrast, negative, epoxy-based photoresist capable of producing microstructures over a wide range of thicknesses [37]. Three layers of SU-8 were processed on a standard 100 mm diameter, 500 μm thick, n-type (100)-oriented silicon wafer as follows. A 200 μm thick film of SU-8 2100 was spin coated, soft baked in a C-005 convection oven (Lindberg/Blue M, Asheville, NC) (95 °C, 55 min), exposed (365 nm, 375 mJ/cm^2), and post exposure baked (95 °C, 25 min). A 10 μm thick film of SU-8 2010 was then spin coated, soft baked (95 °C, 5 min), exposed (100 mJ/cm^2), and post exposure baked (95 °C, 5 min). Next, a 100 μm thick

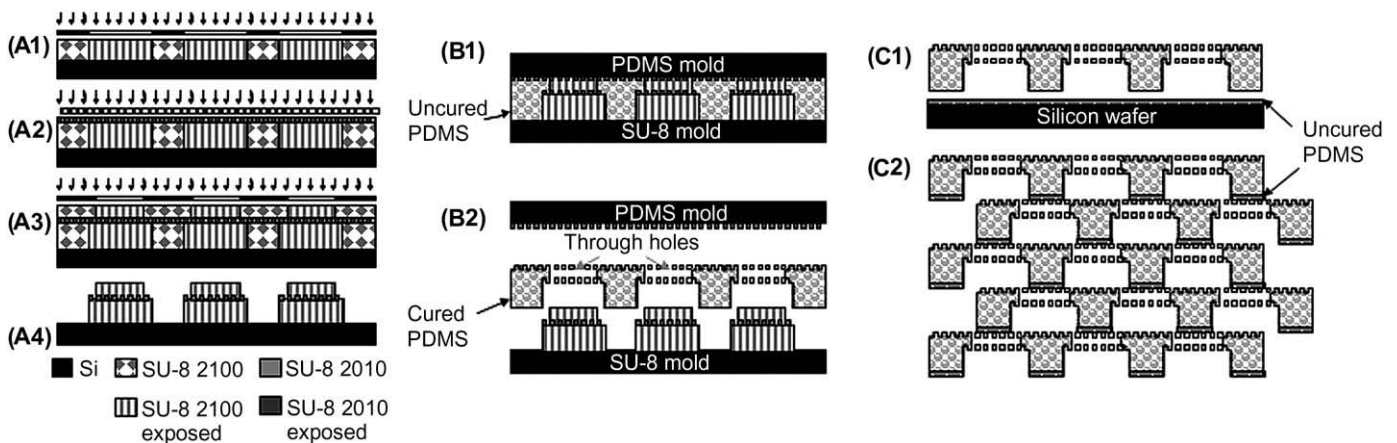**Fig. 1.** Fabrication of 3D PDMS scaffolds. The first step is the processing of multilevel SU-8 molds starting with patterning of a 200 μm thick layer of SU-8 2100 (A1) followed by patterning of a 10 μm thick layer of SU-8 2010 (A2), and patterning of a 100 μm thick layer of SU-8 2100 (A3). All three layers were developed at the same time with SU-8 Developer to dissolve the un-exposed regions (A4). The second step consists of dual-sided molding of PDMS. Images illustrate the two aligned molds in contact with each other while squeezing and molding PDMS (B1); and the cured PDMS layer released from the molds (B2). The third step in the fabrication is stacking of the PDMS layers. Images depict stamping of a PDMS layer over a 10 μm thick uncured PDMS film (adhesive) to wet the tips of the 200 μm diameter columns (C1); and subsequent stacking of layers to achieve a meandering pore geometry (C2). Curing of the adhesive PDMS resulted in adhesion of all the PDMS layers to realize a 3D scaffold with 66% porosity and 71% of surfaces covered with 10 μm diameter and 10 μm high posts.

film of SU-8 2100 was spin coated, soft baked, exposed, and post exposure baked using the same process parameters as the first film. Finally, all three SU-8 layers were simultaneously developed in SU-8 Developer (MicroChem Corp.) (25 °C, 50 min) using agitation, to realize a multilevel SU-8 mold with 200, 10, and 100 μm high features (Fig. 1A).

A second mold was fabricated out of PDMS by spin coating a 10 μm thick film of SU-8 2010 on a standard 100 mm diameter, 500 μm thick, n-type (100)-oriented silicon wafer using the same protocol as the one used for the previous mold. The SU-8 was then developed in SU-8 Developer with agitation for 12 min to realize a surface with 10 μm diameter post micro-textures. Finally, this SU-8 micro-textured surface was used to cast and produce the PDMS mold comprising 10 μm diameter and 10 μm deep holes using a method previously described [29]. This second mold was made of PDMS because its transparency and flexibility facilitate alignment and subsequent separation of the two molds during dual-sided molding of the final PDMS layer.

2.1.2. Dual-sided molding

PDMS was mixed as previously described [29,31], poured on top of both molds, distributed to cover all the patterned areas of the molds, and degassed for 15 min. Then, both molds were placed on a custom mechanical jig, which allows horizontal, vertical, and rotational motion control for alignment of the molds within ~±10 μm [36]. The two molds were then aligned and brought into contact (with the patterned sides facing each other) while squeezing down on the uncured PDMS. The jig is subsequently placed inside an oven at 75 °C for 2 h to cure the PDMS (Fig. 1B).

2.1.3. Stacking of PDMS layers

The patterned PDMS layer specimens were stacked using uncured PDMS as adhesive. PDMS was prepared as explained above, poured to cover a smooth 100 mm diameter, 500 μm thick, n-type (100)-oriented silicon wafer, and spin coated using a *400 Lite* spinner (Laurell Technologies, North Wales, PA) at 4000 revolutions per minute (rpm) to achieve a ~10 μm thick layer. The cured and patterned specimens were stamped on top of the uncured PDMS, so that the tips of the 200 μm columns were wetted with uncured PDMS. Then, the layers were stacked one on top of the other after being aligned with the aid a standard light microscope (Fig. 1C). The aligned and stacked PDMS layers were subsequently baked at 95 °C for 30 min to cure the PDMS (adhesive) and bond the PDMS layers. Lastly, the 3D structures were cut using either a 1 cm diameter circular die to create scaffolds for cell experiments (5 PDMS layers), or a blade to obtain samples for scanning electron microscope (SEM) examination (5–12 PDMS layers).

2.2. CTPs on 3D scaffolds

2.2.1. 3D smooth control

In order to compare the effect of these scaffolds on CTP growth, another set of 3D scaffolds was fabricated with the same steps of mold fabrication, dual-sided molding, and stacking of PDMS layers, with the exception of the 10 μm micro-textures (3D Smooth). This process created 3D scaffolds with exactly the same micro-architecture, but with smooth surfaces instead of micro-textured surfaces.

2.2.2. CTP preparation

Bone-marrow aspirates were harvested with informed consent from 3 patients immediately prior to elective orthopaedic procedures [33,34]. Briefly, a 2 ml sample of bone marrow was aspirated from the anterior iliac crest into 1 ml of saline containing 1000 units of heparin (Vector Labs, Burlingame, CA). The heparinized marrow sample was suspended into 20 ml of Heparinized Carrier Media (alpha-MEM + 2 units/ml Na-heparin; Gibco, Grand Island, NY) and centrifuged at 1500 rpm for 10 min. The buffy coat was removed and resuspended in 20 ml of 0.3% BSA-MEM (Gibco) for subsequent inoculation of the cells on the scaffolds.

2.2.3. 3D scaffold set up and cell inoculation

The 3D Texture and 3D Smooth scaffolds were sterilized for 30 min with 70% ethanol (Aaper Alcohol and Chemical Co.), followed by a triple rinse with phosphate buffered saline (PBS) (Mediatech, Inc. Herndon, VA). Each scaffold was then placed inside of a 10 ml syringe for loading of the cells. Prior to cell inoculation, the cells were diluted in 2.5 ml of α-MEM media (Gibco) with 10% Fetal Bovine Serum (FBS) (Whittaker, Walkersville, MD) plus Dexamethasone (Sigma–Aldrich) [29,30], counted using a hemocytometer, and loaded in a syringe. The syringe was placed on a *NE-500* syringe pump (New Era Pump Systems, Wantagh, NY), which was operated to pass the 2.5 ml of media containing cells at 1.5 ml/min trough the scaffolds. The effluent media and cells were collected and counted to determine the cell-loading efficiency into each scaffold. All scaffolds used to compare cell growth between 3D Texture and 3D Smooth were loaded in this manner. The experiment was repeated three times, using CTPs corresponding to the 3 human donors.

A separate cell culture was set up in order to determine whether cells were able to migrate in a vertical upward direction within the 3D Texture scaffolds. The objective of this particular experiment was not to compare cell growth characteristics on the different scaffolds, but rather to establish whether the CTPs would successfully migrate upwards on the scaffolds. Cells from the same population as those inoculated into the scaffolds were cultured in a glass tissue culture dish (Lab-Tek, Nalge Nunc Int., Naperville, IL). On Day 9, a 3D Texture scaffold was placed on

top of the live cells with the 200 μm columns facing down, so that the tips of these columns were in contact with the cells in culture. This set up was then cultured for another 4 days to investigate whether cells migrated up from the surface of the tissue culture dish into the scaffold.

2.2.4. Cell culture and analysis

After 9 days in culture, cells were stained with 6-diamidino-2-phenylindole dihydrochloride hydrate (DAPI) (Vector Labs) for nuclear fluorescence [29,30]. Other cell-loaded scaffolds were fixed with 2% paraformaldehyde (Electron Microscopy Sciences, Washington, PA) for 10 min, permeabilized for 10 min with 0.2% Triton X-100 (Lab Chem Inc., Pittsburgh, PA). Cells were then stained with Rhodamine Phalloidin (Sigma, St. Louis, MO) at 1:50 in PBS for 45 min at 25 °C for viewing the cytoskeletal actin.

Cell growth was characterized by quantifying the number of CTP progeny per colony in order to investigate proliferation characteristics on the different scaffold surfaces, and account for possible differences in cell-loading efficiency. An epi-fluorescence microscope (Olympus BX50F, Olympus Optical Co.) and confocal microscope (Leica TCS-SP Laser Scanning Confocal Microscope, Heidelberg, Germany) were used to determine the colonies and count the cell number per colony. The cells were counted by taking advantage of the transparency of the PDMS layers and the orthogonality of the micro-architecture (horizontal and vertical walls), which facilitated quantification by focusing the microscopes at different depths of the colonies and counting the cells on the various scaffold levels.

In order to confirm the scaffold effects on cell proliferation, the number of cells per scaffold was measured *via* DNA quantification. CTP-seeded scaffolds were resuspended with a 50 μl of lysis buffer (Sigma–Aldrich) to lyse the membrane of adherent CTP progeny. Stock PicoGreen reagent was diluted 1:200 in TE buffer (Molecular Probes, Eugene, OR) and 1 ml of that was added to each DNA containing sample. The fluorescence was measured with the SpectraMax Gemini fluorescence microplate reader (Molecular Devices Co.; Sunnyvale, CA) at excitation and emission wavelengths of 480 and 520 nm, respectively. Using this analysis, we determined ~4.5 μg of DNA in 1×10^6 adherent CTPs. Thus, we estimated the number of cells for each sample by assuming that 4.5 pg of DNA represents one cell.

Expression of osteoblast specific genes, such as alkaline phosphatase (AP) and osteocalcin (OC) were detected by Reverse Transcription-Polymer Chain Reaction (RT-PCR). Total cellular RNA was isolated with RNAeasy kit (Qiagen Inc., Valencia, CA) and reverse transcribed by conventional protocols with a Sensiscript Reverse Transcription kit (Qiagen Inc). cDNA was then utilized in the PCR kit (USB Co., Cleveland, OH). PCR was used to determine the gene expression of AP, OC, and glyceraldehyde-3-phosphate dehydrogenase (GAPDH). PCR was conducted using an Eppendorf Mastercycler (Eppendorf Co., Westbury, NY). Samples were run on 1.5% agarose gels and photographs were taken with a digital camera. To quantify the mRNA expressions, Gel-Pro Analyzer (Version 3.1; Media Cybernetics, Silver Spring, MD) software was utilized to measure gel band intensities. Relative gene expressions of AP and OC were calculated by dividing band intensities by GAPDH band intensity to obtain numerical results.

2.3. Statistical analysis

The mean and standard deviation values of the experimental data were calculated. All data were subjected to analysis of variance (ANOVA) testing where appropriate (SPSS Inc., Chicago, IL). Significance levels were set at the 95% confidence interval ($p < 0.05$).

3. Results

3.1. Scaffold fabrication

SEM examinations revealed that the three-level SU-8 molds had the desired geometrical dimensions of 200 μm diameter and 200 μm deep holes, 300 μm diameter and 100 μm high columns, and 10 μm diameter and 10 μm deep holes (Fig. 2A). This mold fabrication technique is advantageous because it combines the precision of microfabrication with the complexity and three-dimensionality of multiple SU-8 layering, while using a single developing step. This approach allowed the fabrication of up to six SU-8 levels [37], while reducing overall processing time and avoiding processing complications of coating over patterned surfaces, which would hinder exposure uniformity, feature resolution, and alignment during the dual-sided molding of the PDMS.

SEM observations also revealed PDMS layers ranging between 80 and 120 μm thick, with 300 μm diameter through holes, 10 μm posts on one side of the layer (from the PDMS mold), and 200 μm columns along with 10 μm posts on the other side (from the
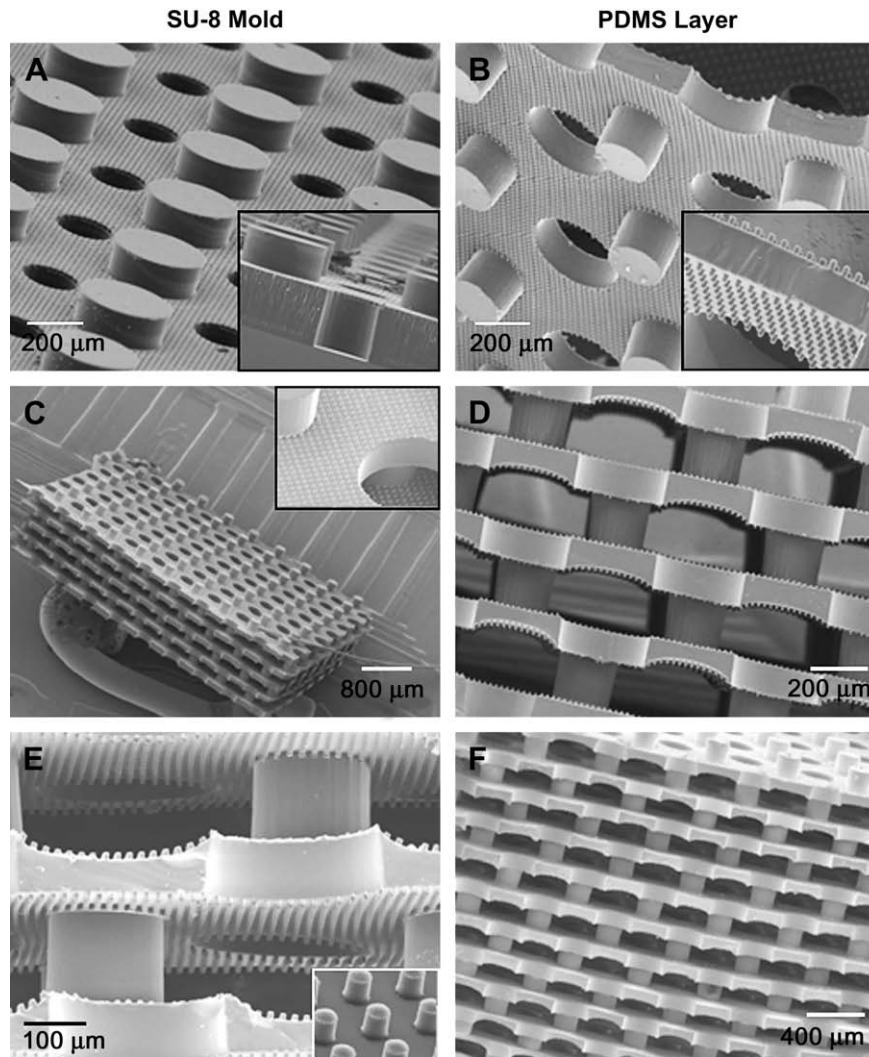
Fig. 2. SEM images show (A) the resulting SU-8 mold with a cross-section (inset), and (B) the dual-sided molded PDMS layer with 300 μm diameter and 100 μm deep through holes, 200 μm diameter and 200 μm high columns, and 10 μm diameter and 10 μm high posts on both sides of the layer (inset). SEM images exemplify (C) a five-layer PDMS scaffold on a penny, (D) a closer view of the cross-section showing the alignment between adjacent layers that resulted in a meandering pore geometry, and (E) 10 μm diameter and 10 μm high posts present on all horizontal surfaces. (F) Scaffold height was increased by adding more PDMS layers.

triple-layer-patterned SU-8 mold) (Fig. 2B). The custom mechanical jig significantly enhanced the alignment of the two molds used for dual-sided molding of the PDMS. In this step, special care was given to ensuring uniform contact between the two molds to avoid blocked through holes and non-uniform thickness of the PDMS layers [36]. The resulting PDMS layers exhibited a ±20 μm variation from the desired 100 μm thick PDMS layer.

Alignment of the PDMS layers was facilitated by the transparency of the PDMS, where the 300 μm diameter through holes and 200 μm diameter columns served as alignment marks during the stacking step with a resulting alignment accuracy of ±30 μm between the stacked PDMS layers. Stamping uncured PDMS onto the 200 μm columns as adhesive was a convenient way to attach the different layers. However, care was necessary to assure a uniform stamping/wetting of the tips of these columns, as well as subsequent contact between PDMS layers during stacking. If the 200 μm diameter columns of the PDMS layers were brought into contact unevenly with the uncured PDMS (adhesive), over-wetting of some columns would result, which, in turn, could lead to destruction of nearby micro-textures [36].

Fig. 2C–E presents a 5 layer 3D Texture scaffold, which exhibits 66% porosity by volume with 300 μm diameter meandering vertical pores, 200 μm × 400 μm horizontal pores, and 71% of the surfaces within the scaffold covered with 10 μm diameter and 10 μm high posts. The height (three-dimensionality) of the resulting 3D scaffolds can be increased by simply stacking more PDMS layers (Fig. 2F).

3.2. CTPs within the 3D scaffolds

The effect of the 10 μm diameter and 10 μm high posts, with 10 μm separation, on CTP behavior was investigated by culturing CTPs on the 3D Texture and 3D Smooth scaffolds. Cells attached, migrated, proliferated, and differentiated in all three dimensions on the different features of the micro-architecture within the scaffolds. CTP colonies were visible on different levels of both 3D Texture and 3D Smooth scaffolds, with cells growing from the top surface down to 4 PDMS layers deep per colony (Fig. 3). These observations suggest that in the vertical direction, cells proliferated and migrated to cover distances of up to ~1.2 mm long, while some colonies reached diameters of ~3.0 mm long in the horizontal direction. Cells were

able to successfully migrate vertically upward as revealed by cells growing from the surface of the tissue culture dish into the 3D Texture scaffold. Cells in different colonies were visible growing on the top and bottom of each PDMS layer, on the walls of the 300 μm pores, and on the 200 μm columns linking the different PDMS layers (Fig. 3). In addition, confocal microscope images exhibited a clear actin cytoskeleton that appeared to grow within and around the posts (Fig. 3F).
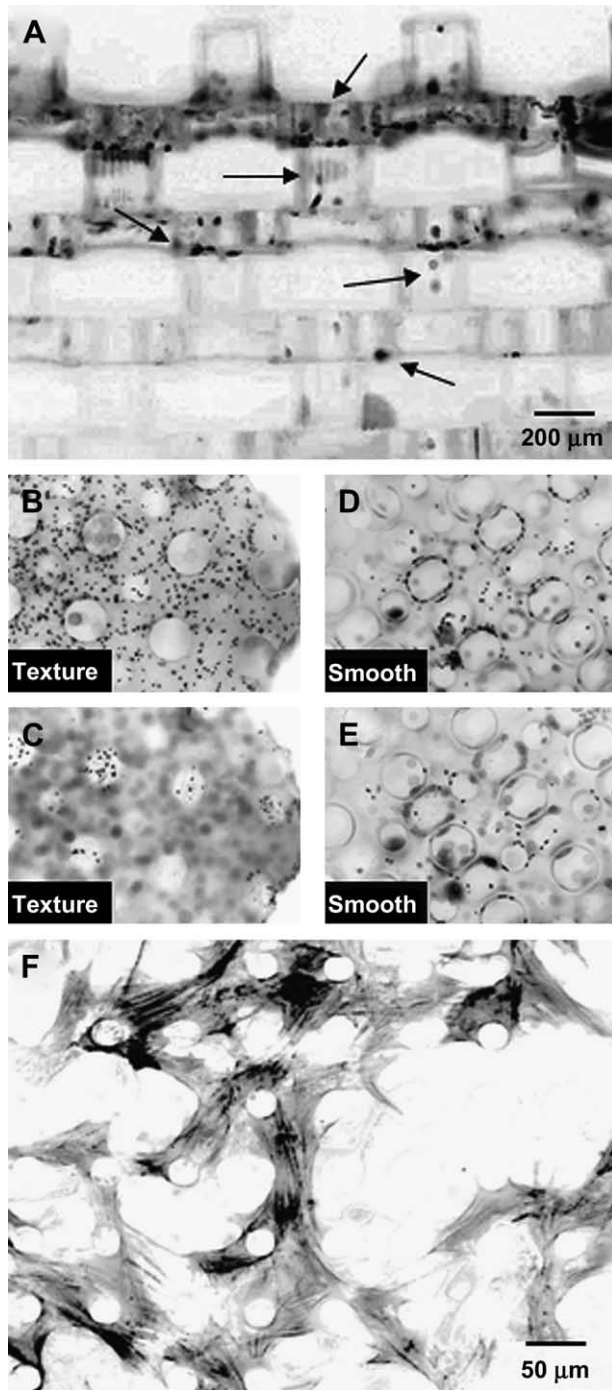

Fig. 3. Immunofluroscent microscope images depict (A) a side-view cross-section of a 3D Texture scaffold with cells growing on 4 PDMS levels of the scaffold; a top-view of cells growing on (B, C) 3D Texture scaffolds, which consistently showed bigger colonies than cells on (D, E) 3D Smooth scaffolds; and (F) cells growing on a 3D Textures scaffold exhibiting a well-defined actin cytoskeleton located within and around the posts. *Note: the original color images were converted to grayscale and reversed to provide visual clarity.*

On the first two experiments, cell-loading efficiency was similar on both 3D Texture (47%, 80%) and 3D Smooth (60%, 74%) scaffolds (Table 1). On the third experiment, 3D Texture (4%) had considerably less number of cells attached to it compared to cells on 3D Smooth (30%). We attributed this lower cell-loading efficiency on 3D Texture to mechanical shifting of the scaffold during cell loading, and from air bubbles trapped within the scaffold that blocked passing and subsequent loading of cells. Nevertheless, we considered this experiment as part of our investigation since we are not evaluating the loading capacity of the scaffolds, and the cell quantification is presented as cell number per colony, which should account for differences in loading efficiency. The 3D Texture scaffolds consistently presented more cells per colony than 3D Smooth (Fig. 4) for all three experiments. For the three experiments (cells from three patients), the 3D Texture scaffolds exhibited 443, 645, and 470 cells per colony, while the 3D Smooth scaffold exhibited 162, 194, and 203 cells per colony. The data from the three experiments were pooled to account for the effects of known CFU variation [38]. Analysis of this collective data resulted in a mean cell number per colony of 499 for 3D Texture compared to 188 cells per colony on 3D Smooth, which represents a statistically significant difference ($p < 0.05$) between the two types of scaffolds. This increasing cell number per colony is also supported by the DNA quantification analysis. In three experiments (cells from three patients), 3D Texture scaffolds (mean cell number of 239,012) supported a greater number of CTP progeny ($p < 0.05$) compared to 3D Smooth ones (mean cell number of 154,153). Expression of key osteoblastic bone markers, such as AP and OC in the CTP progeny on each scaffold was evaluated using RT-PCR (Fig. 5). AP mRNA expression was significantly higher ($p = 0.002$) on the 3D Texture relative to 3D Smooth scaffolds. Similarly, OC mRNA expression was also higher on 3D Texture scaffolds, but this difference was not statistically significant ($p = 0.059$).

4. Discussion

The scaffold micro-architecture and surface micro-textures play a key role in the development of specific biological functions [9,39]. Although it is inherently a 2D technique, microfabrication offers a unique opportunity to precisely control the physical microenvironment of cells and tissues with high resolution and reproducibility. Taking advantage of these characteristics, several groups have developed 3D scaffolds with precise micro-architecture tailored to guide tissue growth in well-defined configurations [18–22,40]. Nonetheless, despite clear evidence that surface micro-textures can modulate cell and tissue behavior [23–31], only recently are groups attempting to incorporate precise and bioactive surface topographies within the pores of precisely defined 3D micro-architectures for tissue engineering applications [22]. Therefore, the fabrication technique reported here presents a unique approach to integrate well-defined micro-architectures with precise surface micro-textures engineered to specifically guide the growth of different cells and tissues. The main advantage

Table 1
Loading efficiency and colony number.

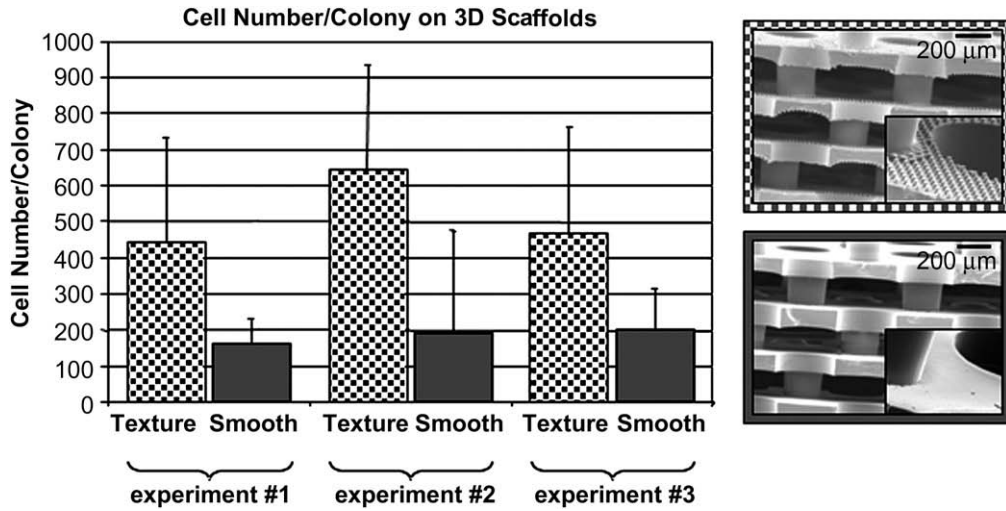|	Scaffold	Cell loading (%)	Colony number
Exp 1	Texture	47	9
	Smooth	60	9
Exp 2	Texture	80	5
	Smooth	74	4
Exp 3	Texture	4	8
	Smooth	30	14

Fig. 4. Graph summarizes the mean cell number/colony quantification from all three experiments on both 3D Texture (top inset image) and 3D Smooth (bottom inset image) scaffolds. Cells growing on 3D Texture scaffolds consistently formed bigger colonies than cells on the 3D Smooth scaffolds in all three experiments.
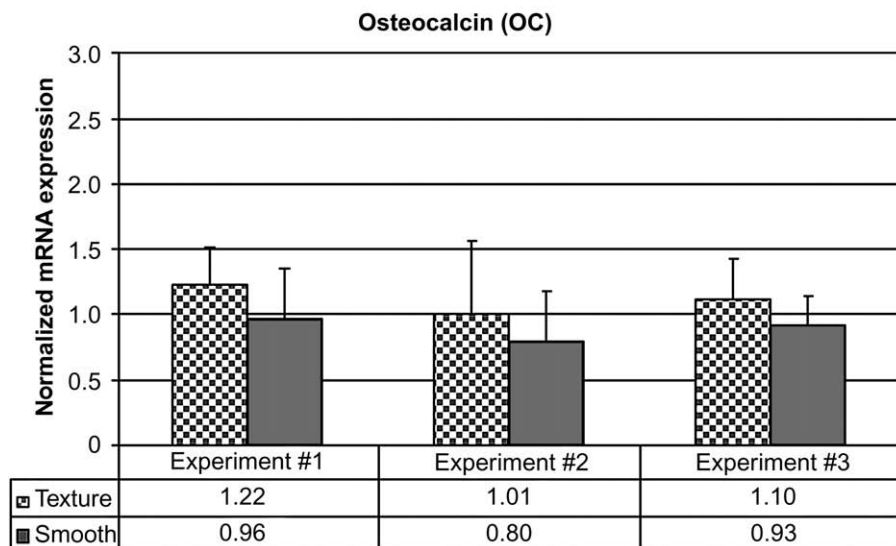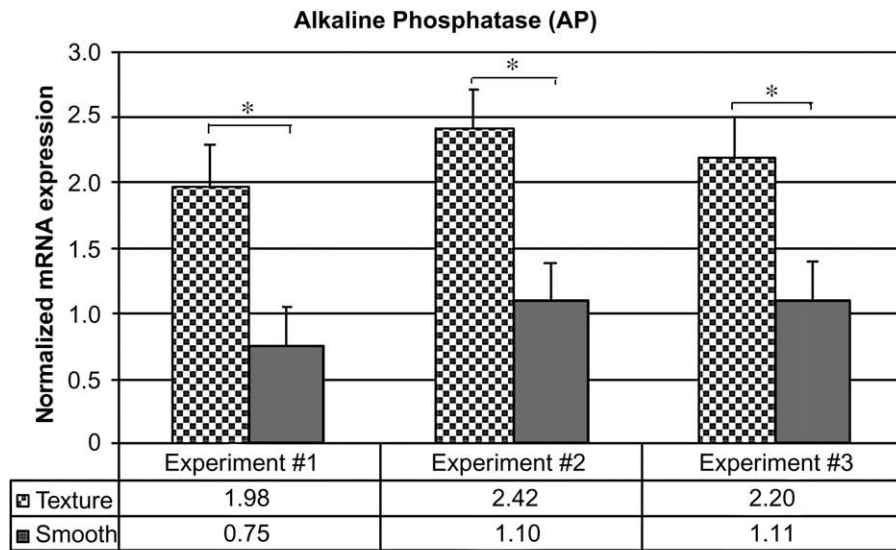

	Experiment #1	Experiment #2	Experiment #3
▨ Texture	1.98	2.42	2.20
▦ Smooth	0.75	1.10	1.11

	Experiment #1	Experiment #2	Experiment #3
▨ Texture	1.22	1.01	1.10
▦ Smooth	0.96	0.80	0.93

Fig. 5. Expression of the key osteoblastic bone markers, such as AP and OC, was assessed in the CTP progeny on each scaffold using RT-PCR. AP mRNA was expressed more strongly on 3D Texture ($p = 0.002$) relative to 3D Smooth scaffolds. OC mRNA expression was also higher on 3D Texture, but not significant ($p = 0.059$), compared to 3D Smooth scaffolds.

of this approach is that it permits the fabrication of 3D scaffolds with hierarchical geometrical resolution, starting from a few microns to selectively interact with individual cells, up to hundreds and thousands of microns to guide large groups of cells and tissues. In this manner, it may be possible to promote particular biological responses solely through selective physical stimuli and without destabilizing the delicate biochemical environment. Furthermore, the inherent precision and reproducibility of microfabrication allows not only small geometrical modifications to better identify and quantify specific effects on cell behavior, but also to optimize these geometrical features to enhance and direct specific cell behaviors and tissue growth, respectively. The fabrication method presented here enables the incorporation of such topographical patterns on well-defined interconnected pores within 3D scaffolds.

Within the field of tissue engineering, the need to treat and increase the functionality and quality of life of an aging world population demands novel and efficient therapies to promote bone regeneration [6]. Our approach, which is generic and can be used to create tissue engineering scaffolds with potential use in a variety of human tissues, was specifically tailored to evaluate its potential in bone tissue engineering. The *in vitro* cell culture results reported here support the hypothesis that 3D scaffolds can be fabricated with precise micro-architecture and surface micro-textures designed to stimulate CTPs. First, the scaffolds allowed attachment of CTPs within the 3D space. Next, the 300 μm diameter vertical meandering pores and 200 μm × 400 μm horizontal pores enabled CTPs to grow and migrate in three dimensions within the scaffold, which is a critical step in bone cell survival and subsequent bone formation [31]. Cells were observed to adhere initially in different locations within the scaffold, as well as migrate and proliferate on both the horizontal micro-textured surfaces and the vertical columns that linked the different PDMS levels (Fig. 3A). This adhesion, migration, and proliferation led to the formation of distinct 3D CTP colonies that expanded both horizontally and vertically within the scaffold. The observed 3D cell colonization and distribution within a scaffold is a critical component for promoting key biological processes like cell communication, vascularization, hydroxyapatite formation [6,16], and the engineering of a functional bone tissue. Our fabrication approach permits the development of well-defined pores of specific size and shape within this 3D space, that is designed for optimum bone tissue in-growth [10,11]. Finally, the 10 μm diameter and 10 μm high posts significantly enhanced the growth of CTPs (without compromising their early differentiation process as observed from the AP and OC mRNA expression) compared to smooth surfaces, as had been previously reported for 2D substrates *in vitro* [30]. Although CTP colonies were observed on both topographically patterned and non-topographically patterned 3D scaffolds, the micro-architecture and surface micro-textures of the 3D Texture scaffold provided superior osteoconductive-like (migration and proliferation) stimuli compared to the 3D Smooth scaffold. However, these are preliminary results, which must be interpreted with care, and although osteoblastic phenotype appears to be enhanced, further experimentation is required to report more conclusive results on the scaffold's effect on cell differentiation. Nonetheless, enhancement of CTP growth, within a 3D environment, based solely on precise porosity and surface topographical features, represents significant improvement and potential for the engineering of functional tissues like bone. This data proves the feasibility of our 3D microfabrication approach and demonstrates the possibility to control, guide, and enhance cell growth with such physical stimulation.

In the 3D Texture scaffolds, the 10 μm diameter and 10 μm high posts significantly enhanced the proliferation of CTPs in both horizontal and vertical directions. Colonies formed by these cells were observed to expand up to four PDMS layers, demonstrating 3D migration and colonization as well as CTP interconnectivity throughout the scaffold (Fig. 3A). Although CTP colonies expanded through different PDMS layers, the majority of cells were observed to grow primarily on the surfaces where the post micro-textures were available, which is consistent with previous data [32] that demonstrates an affinity of these cells to grow within the posts. Therefore, it would be advantageous to maximize the amount of surface area covered by these posts within the scaffold. However, there are several parameters that limit the amount of surface area available to be patterned with the 10 μm posts. First, the scaffold fabrication process does not readily allow for patterning on vertical surfaces. Therefore, it may be desirable to minimize the amount of vertical surface area within the scaffold. Second, there is a trade off between increasing the amount of horizontal surface area covered in these 10 μm posts, and increasing the overall porosity of the scaffold. The more horizontal area there is available to pattern, the lower the overall scaffold porosity, which is another important parameter to maximize. The 3D Texture scaffolds were designed to have an overall scaffold porosity of 66% (by volume), and the surface area covered with 10 μm post textures at 71% (100% of horizontal surface area), which could be easily modified by changing the sizes and shapes of patterns on the photomasks used during the mold fabrication step. It is important to keep in mind that although this fabrication method would allow us to further increase the current scaffold porosity, there is a limitation to the overall porosity we can achieve due to inherent fabrication and material characteristics. However, based on the current results, it is tempting to speculate that the ability to control the surface topography and pore uniformity may be as (or perhaps more) efficient in promoting cell and tissue growth than the increased porosity offered by alternative fabrication techniques such as solvent casting. Although PDMS has been used in a variety of tissue engineering applications [2–4,32] and has served as a model material to demonstrate the feasibility of this fabrication technique, it would be beneficial to translate this fabrication technique to other biodegradable materials. As a possible direction for future research, we speculate that the fabrication processes reported here would permit the use of alternative materials such as poly(glycerol sebacate) [41], poly-caprolactone [42], and poly(lactic-co-glycolic acid) [43], which have been topographically patterned in 2D using similar processes. Nonetheless, the optimum conditions of porosity, pore uniformity, surface topography, and material may depend on the type of therapeutic application (for example *in vitro* or *in vivo*, types of cells, etc.).

From the cell number per colony and DNA quantification results, the 3D Texture scaffolds significantly enhanced CTP proliferation. This increase in CTP proliferation did not result in a decrease in osteoblastic differentiation as was evident from the mRNA expression of AP and OC [44–46]. Moreover, AP mRNA expression was significantly stronger on 3D Texture compared to 3D Smooth scaffolds. AP is an earlier marker of osteoblastic differentiation while OC is a later one [46]. Therefore, the cells growing on 3D Texture appear to exhibit an increase in early osteoblastic differentiation, which is evident by a higher expression of the AP gene, but not yet observable by OC gene expression. Obviously, more experiments are needed to conclude a possible increase in CTP differentiation. Nonetheless, these results demonstrate that the 3D Texture scaffolds are likely enhancing CTP proliferation without diminishing their osteoblastic differentiation.

5. Conclusions

The present study describes an innovative technique to fabricate 3D scaffolds with both precise micro-architecture and surface micro-textures designed to osteoconductively direct CTPs. This process allowed the fabrication of a 3D Texture scaffold with 66%

porosity by volume that consisted of 300 μm diameter meandering vertical pores, 200 μm × 400 μm horizontal pores, and 71% of the surfaces within the scaffold covered with 10 μm diameter and 10 μm high posts. The 3D scaffold allowed cells to attach, migrate, and proliferate more osteogenically compared to those on scaffolds with smooth surfaces. These results collectively support the possibility of creating tissue engineering scaffolds capable of inducing specific bioactive responses based on physical stimuli provided by the micro-architecture and the surface micro-textures. Furthermore, the fabrication technique easily permits modification of this micro-architecture and surface micro-textures to be optimally designed for specific cells and tissues.

Acknowledgements

References

[1] Stupp SI. Biomaterials for regenerative medicine. MRS Bull 2005;30(7):546–53.
[2] Khetani SR, Bhatia SN. Engineering tissues for in vitro applications. Curr Opin Biotechnol 2005;17:524–31.
[3] Khademhosseini A, Langer R, Borenstein J, Vacanti JP. Microscale technologies for tissue engineering and biology. PNAS 2006;103:2480–7.
[4] Norman JJ, Desai TA. Control of cellular organization in three dimensions using a microfabricated polydimethilsoloxane-collagen composite tissue scaffold. Tissue Eng 2005;11:378–86.
[5] Norman JJ, Collins JM, Sharma S, Russell B, Desai TA. Microstructures in 3D biological gels affect cell proliferation. Tissue Eng 2008;14(3):379–90.
[6] Salgado AJ, Coutinho OP, Reis RL. Bone tissue engineering: state of the art and future trends. Macromol Biosci 2004;4:743–65.
[7] Tsang VL, Bhatia SN. Three-dimensional tissue engineering. Adv Drug Deliv Rev 2004;56:1635–47.
[8] Hutmacher DW. Scaffolds in tissue engineering bone. Biomaterials 2000;21:2529–43.
[9] Shieh M. Control of bone cell functions on three-dimensional tissue engineering scaffolds. BUG J 2000;3:194–204.
[10] Liu DM. Fabrication of hydroxyapatite ceramic with controlled porosity. J Mater Sci Mater Med 1997;8:227–32.
[11] Chu TMG, Halloran W, Hollister SJ, Feinberg SE. Hydroxyapatite implants with designed internal architecture. J Mater Sci Mater Med 2001;12:471–8.
[12] Berry CC, Campbell G, Spadiccino A, Curtis ASG. The influence of microscale topography on fibroblast attachment and motility. Biomaterials 2004;25:5781–8.
[13] Borden M, Attawia M, Khan Y, Laurencin CT. Tissue engineering microsphere-based matrices for bone repair: design and evaluation. Biomaterials 2002;23:551–9.
[14] Gabriel-Chu TM, Feinberg SE, Halloran JW. Mechanical and in vivo performance of hydroxyapatite implants with controlled architectures. Biomaterials 2002;23:1283–93.
[15] Yang S, Leong KF, Du Z, Chua CK. The design of scaffold for use in tissue engineering. Part II. Rapid prototyping techniques. Tissue Eng 2002;8:1–11.
[16] Ma PX. Scaffolds for tissue fabrication. Mater Today 2004;7:30–40.
[17] Leong KF, Cheah CM, Chua CK. Solid freeform fabrication of three-dimensional scaffolds for engineering replacement tissues and organs. Biomaterials 2003;24:2363–78.
[18] Vozzi G, Flaim C, Ahluwalia A, Bhatia S. Fabrication of PLGA scaffolds using soft lithography and microsyringe deposition. Biomaterials 2003;24:2533–40.
[19] Mattioli-Belmonte M, Vozzi G, Kyriakidou K, Pulieri E, Lucarini G, Vinci B, et al. Rapid-prototyped and salt-leached PLGA scaffolds condition cell morphofunctional behavior. J Biomed Mater Res A 2007;85A:466–76.
[20] Folch A, Mezzour S, During M, Hurtado O, Toner M, Muller R. Stacks of microfabricated structures as scaffolds for cell culture and tissue engineering. Biomed Microdevices 2000;2:207–14.
[21] Papenburg BJ, Vogelaar L, Stamatialis DF, Wessling M. One step fabrication of porous micropatterned scaffolds to control cell behaviour. Biomaterials 2007;28:1998–2009.
[22] Seunarine K, Meredith DO, Riehle MO, Wilkinson CDW, Gadegaard N. Biodegradable polymer tubes with lithographically controlled 3D micro- and nanotopography. Microelectron Eng 2008;85:1350–4.
[23] von Recum AF, Shannon CE, Cannon CE, Meyle J. Surface roughness, porosity, and texture as modifiers of cellular adhesion. Tissue Eng 1996;2:241–53.
[24] Curtis A, Wilkinson C. Topographical control of cells. Biomaterials 1998;18:1573–83.
[25] Singhvi R, Stephanopoulos G, Wang DIC. Effects of substratum morphology on cell physiology. Biotechnol Bioeng 1994;43:764–71.
[26] Xia Y, Whitesides GM. Soft lithography. Ann Rev Mater Sci 1998;28:153–84.
[27] Desai TA. Micro- and nanoscale structures for tissue engineering constructs. Med Eng Phys 2000;22:595–606.
[28] Chesmel KD, Clark CC, Brighton CT, Black J. Cellular responses to chemical and morphologic aspects of biomaterial surfaces. II. The biosynthetic and migratory response of bone cell population. J Biomed Mater Res 1995;29:1101–10.
[29] Mata A, Boehm C, Fleischman A, Muschler G, Roy S. Analysis of connective tissue progenitor cell behavior on polydimethylsiloxane smooth and channel micro-textures. Biomed Microdevices 2002;4:267–75.
[30] Mata A, Boehm C, Fleischman A, Muschler G, Roy S. Growth of connective tissue progenitor cells on micro-textured polydimethylsiloxane surfaces. J Biomed Mater Res 2002;62:499–506.
[31] Mata A, Su X, Fleischman A, Roy S, Banks B, Miller S, et al. Osteoblast attachment to a textured surface in the absence of exogenous adhesion proteins. IEEE Trans Nanobioscience 2003;2:287–94.
[32] Mata A, Boehm C, Fleischman A, Mushcler G, Roy S. Connective tissue progenitor cell growth characteristics on textured substrates. Int J Nanomedicine 2007;2:1–18.
[33] Muschler G, Midura R, Nakamoto C. Practical modeling concepts for connective tissue stem cell and progenitor compartment kinetics. J Biomed Biotechnol 2003;3:170–93.
[34] Muschler G, Nitto H, Matsukura Y, Boehm C, Valdevit A, Kambic H, et al. Spine fusion using cell matrix composites enriched in bone marrow derived cells. Clin Orthop 2003;407:102–18.
[35] Muschler G, Nakamoto C, Griffith L. Engineering principles of clinical cell-based tissue engineering. J Bone Joint Surg Am 2004;86:1541–58.
[36] Mata A, Fleischman A, Roy S. Microfabricated 3D scaffolds for tissue engineering applications. Mater Res Soc Symp Proc 2005;845:AA4.3.1–4.3.7.
[37] Mata A, Fleischman A, Roy S. Fabrication of multi-layer SU-8 microstructures. J Micromech Microeng 2006;16:276–84.
[38] Muschler G, Boehm C, Easley K. Aspiration to obtain osteoblast progenitor cells from human bone marrow: the influence of aspiration volume. J Bone Joint Surg Am 1997;79:1699–709.
[39] Silva GA, Czeisler C, Niece KL, Stupp SI. Selective differentiation of neural progenitor cells by high-epitope density nanofibers. Science 2004;303:1352–5.
[40] Shin M, Matsuda K, Ishii O, Terai H, Kaazempur-Mofrad M, Borenstein J, et al. Endothelilized networks with a vascular geometry in microfabricated poly-(dimethyl siloxane). Biomed Microdevices 2004;6:269–78.
[41] Bettinger CJ, Orrick A, Misra A, Langer R, Borenstein JT. Microfabrication of poly(glycerol-sebacate) for contact guidance applications. Biomaterials 2006;27:2558–65.
[42] Sarkar S, Lee GY, Wong JY, Desai TA. Development and characterization of a porous micro-patterned scaffold for vascular tissue engineering applications. Biomaterials 2006;27:4775–82.
[43] Owen GR, Jackson J, Chehroudi B, Burt H, Brunette DM. A PLGA membrane controlling cell behaviour for promoting tissue regeneration. Biomaterials 2005;26:7447–56.
[44] Catelas I, Sese N, Wu B, Dunn J, Helgerson S, Tawil B. Human mesenchymal stem cell proliferation and osteogenic differentiation in fibrin gels in vitro. Tissue Eng 2006;12(8):2385–96.
[45] Madras N, Gibbs A, Zhou Y, Zandstra P, Aubin J. Modeling stem cell development by retrospective analysis of gene expression profiles in single progenitor-derived colonies. Stem Cells 2002;20:230–40.
[46] Lian JB, Stein GS, Stein JL, van Wijnen AJ. Osteocalcin gene promoter: unlocking the secrets for regulation of osteoblast growth and differentiation. J Cell Biochem Suppl 1998;90:3162–6.